Thermal Modeling of the FZG Test Rig: Application to Starved Lubrication Conditions

Pierre Navet, Christophe Changenet, Fabrice Ville, Dhafer Ghribi, Jérôme Cavoret

Thermal modelling of the FZG test rig: application to starved lubrication conditions

P. Navet[1;2;3], C. Changenet [2], F. Ville[1], D. Ghribi[3], J. Cavoret[1]

[1]Univ Lyon, INSA-Lyon, CNRS UMR5259, LaMCoS, F-69621, France

[2]Univ. Lyon, ECAM Lyon, LabECAM, Lyon, France

[3]Safran Transmission Systems, Colombes, France

Corresponding author F. Ville fabrice.ville@insa-lyon.fr

Abstract

During their lifetime, gears may undergo starved lubrication operating conditions. Starvation condition has an impact on friction between gears that leads to modify gearbox efficiency. In this paper, lubricant starvation tests on an FZG test rig adapted to this condition are presented. Gears were equipped with embedded thermocouple sensor to measure their operating bulk temperature. An experimental method to isolate test box power loss of FZG machine is proposed. A thermal model of this test rig draws up the power loss distribution into the test box for a nominal condition of lubrication. At last, a numerical method based on experimental results is proposed to estimate gear power loss variation during lubricant starvation.

Keywords FZG test rig, starvation condition, gear power loss, gear bulk temperature, thermal analysis, thermal network method

Introduction

During their lifetime, gears may undergo starved lubrication operating conditions. Starvation condition has an impact on friction between gears that leads to modify gearbox efficiency. Thermal characterization of gears is usually based on the equilibrium between power loss sources and heat dissipation (1). A significant number of experimental studies on gear efficiency and thermal behaviour have been performed on back-to-back gear test rig. Impact of the lubrication method on efficiency and temperature of spur gears is studied by comparing dip and spray lubrication (2). Fernandes *et al.* (3) modelled power loss of the FZG test rig

under steady-state operating conditions to estimate experimentally the friction coefficient between gears. Another formulation of friction coefficient derived from FZG tests (4) based on Michaelis *et al*. formulation (5) is used in a global scuffing criteria (6). A thermal model of the FZG test rig has been built to study gear power loss (7, 8). In those studies, gear temperatures are considered equal to oil sump one. However, to estimate more accurately the gearbox efficiency, local temperature variation has to be modelled (9). A thermal modelling of the FZG test rig built with the thermal network method is able to determine the bulk temperature of gears for oil bath lubrication condition (10). Thus, a power loss distribution for lubricated conditions is estimated. However, none of these studies focused on starved lubrication condition. Most of studies concerning lubricant starvation focus on point and elliptical contacts that are more representatives of contacts within rolling element bearings. Chevalier *et al*. (11) characterize numerically the degree of starvation of EHL point contacts with the amount of oil present on the surfaces at the contact inlet. This formalism was extended to elliptical contacts (12). Impact of starvation on contact fatigue was studied by Querlioz *et al*. (13).

The aim of this paper is to study the impact of starved lubrication conditions on gear power loss. Firstly, the FZG test rig and the operating conditions are described. In the second part, an experimental method to isolate power loss of the test box is proposed. In the third part, a starvation test performed on a FZG test rig adapted to these conditions is presented. Then, a thermal model of the test rig is built in order to draw up the power loss distribution into the test box for a nominal condition of lubrication. At last, gear power loss variations during starvation are estimated using a numerical method based on experimental results and the thermal model of the FZG test rig adapted to starved condition.

FZG test rig description

Figure 1 presents the FZG test rig machine. This machine is a back-to-back test rig composed of a test box #1 and a slave box #2 both assembled with cylindrical gears. A clutch #3 permits to apply the desired load in the closed loop by torsion of the pinion shaft with a known mass suspended at a lever arm. Thanks to the closed mechanical loop, the motor #4 only ensure kinematics of the system and give mechanical power to compensate power losses. A torque transducer on motor shaft allows to measure total torque loss (Table 1). This FZG test rig is equipped with thermocouple sensors (K type, absolute accuracy of 1.5°C) on fixed parts: housings, oil baths and external ring of rolling element bearings (REB).

FZG C30 gears (Table 2) are used for both boxes. Four 6406 bearings are mounted in each gearbox (Table 3). Those are lubricated with an oil bath of a gearbox oil (Table 4, IGOL HYPOID 85W-90) at the level H1 represented on Figure 2.

In this study, one operating condition (Table 5) is selected. The torque applied on pinion is 60.8 Nm (load stage 4 according to standard FZG classification). The rotational speed of the motor is 2000 rpm (3000 rpm at pinion shaft). All the presented tests were started at ambient temperature and no thermal regulation of oil is performed. Thus, each temperature variation comes from power loss generation of the system.

Repeatability tests were performed to verify the measurement reliability of the loss torque measurement (Figure 3). A maximum difference of 0.3 N.m and an average difference of 0.1 N.m on loss torque are observed. The loss torque measurements are therefore repeatable.

Experimental method to estimate the test box power loss

In order to study more specifically the test box, it is necessary to isolate its power loss. One remembers that only the total torque loss of the system can be measured with the torque transducer on the motor shaft. To isolate the test box power loss, the slave box has to be characterized. The two gearboxes of the machine are mounted similarly. The ventilation of the

motor is blocked by a wood plate in order to ensure a better thermal symmetry of the machine. Symmetry is verified by comparing the temperature profile of the two oil baths during a test under symmetrical conditions (Figure 4). A maximal difference of 0.3 °C is observed between the two oil baths which allows to consider the machine as symmetrical. Thus, power losses are evenly distributed between the two boxes that permits to estimate the slave box power loss as the half of total power loss. Figure 5 shows the profile of the slave box torque loss depending on its oil bath temperature. Torque loss can be accurately approximated by a third-degree polynomial function. In this study, the slave box configuration is fixed and so this characterization can be applied on tests for which the test box is mounted with a different configuration. The torque loss of the test box is estimated by subtracting the slave box loss torque from the total torque loss. This method will be used later to isolate the test box power loss for an asymmetrical configuration of the FZG adapted to starvation tests.

Tests on FZG test rig adapted to lubricant starvation

In a context of oil bath submerging largely gears (level H1, Figure 2), gear bulk and oil sump temperatures are close (9). However, for marginal lubrication conditions like low oil bath level (level H2, Figure 2) or when starvation occurs, temperature elevation of gears has to be taken into account to estimate more accurately their associated power loss. In order to measure gear bulk temperatures, thermocouple sensors (K type) were stuck directly on the tooth side of the pinion and of the wheel (Figure 6). Hollow shafts were designed in order to route wires to the data loggers. Those are directly fixed to the output of the two shafts (Figure 7). Figure 8 gives embedded gears bulk temperatures and oil bath temperature. Pinion operating temperature is almost 20 °C higher than the oil bath one. This thermal elevation is explained by the low oil level which thermally insulates the pinion from oil cooling.

For starvation tests, the test box was assembled with FZG A20 gears (Table 2). Those gears are largely used in works focusing on scuffing. In fact, their profile shift modifications were chosen to induce an exacerbated sliding speed at the recess. Four greased and sealed REB (Table 3, 6306-2RS1) were mounted within the test box. The grease will ensure lubrication of REB during starved conditions.

The test box is lubricated with a base oil (Table 5; Nycobase 5750) at the low level H2 (Figure 2). This level will prevent washing of the REB grease during lubricated phase. Base oil was chosen in order to focus on the impact of rheological parameters of oil and not to observe the chemical influence of additive package on friction like tribofilm formation (17).

Figure 8 shows the repeatability of embedded gears bulk temperatures and the oil bath temperature during the lubricated phase. The maximal difference of the temperature observed is 1 °C and the average difference is 0.2 °C. Temperature measurements are therefore repeatable.

The procedure performed for a starvation test is:

(1) To perform a test under lubricated regime (operating condition 1) until loss torque is considered almost constant (torque loss measurement does not vary over a range of 0.1 N.m during 5 minutes).
(2) To drain the oil bath out of the test box while temperature of each mechanical part drops to ambient temperature.
(3) To perform a starvation test on residual oil. The test has to be stopped in case of critical increase of torque that could damage the transducer.

Figure 9 shows differences between gear bulk temperatures during lubricated and starved test. A thermal kinetics acceleration is observed without oil. In fact, an increase of more than 60 °C on bulk temperatures are measured after 3 minutes (more than 140 %). This increase is due

to the fact that no thermal energy can be collected by oil. Figure 10 presents the difference between the total power loss during lubricated and starved condition. Comparing to nominal lubricated conditions, an increase of 800 W after 3 minutes on the total power loss (60 %) is observed. Focussing on the test box power loss using the experimental method described in part 2, the increase of the power loss described above is observable (Figure 11). It confirms that it comes from the test box. Because REB are lubricated by their grease, one can suggest that the increase of power loss in the system may come from an increase of gear tooth friction.

FZG thermal modelling for oil bath lubrication condition

In order to analyse the dissipation sources which may explain the torque evolution presented in Figure 11, a thermal model of the test gearbox was developed. Thermal modelling of transmission systems was led by Changenet *et al*. (9) using the thermal network method. This method consists in performing a discretization of the transmission system into isothermal elements at mechanical part scale (bearings, gears, shafts, oil, etc). These elements are connected by thermal resistances defined by an analogy of Ohm's law.

Durand de Gevigney *et al*. (10) proposed a thermal modelling of the FZG test rig for oil bath lubrication condition. On Figure 12, a representation of the thermal network is given showing elements, thermal resistances and heat sources of the model. In order to evaluate heat exchanges, the model uses four types of thermal resistance:

(1) Convection and radiation are respectively based on Newton's and Stefan-Boltzmann's laws. Housings are assimilated to a plate assembly. This simplification permits to apply classic laws of plates submitted to normal and tangential air flux (9).

(2) Convection with oil is modelled by laws derived from classical formulation of surfaces submitted to oil flow (11). Heat transfers between the oil bath and internal surfaces of housings are modelled using the forced convection on flat plates. Heat transfer between gears and oil is modelled using rotating disk law.

(3) Conduction is calculated with classic formulations of heat transfer by conduction. Bearing rings, shafts and gears are considered as cylindrical elements in order to apply radial conduction law (9).

(4) Striction thermal resistance is based on Blok's work (15). Heat generated due to friction in gear and REBs contacts are localized on a small area compared to their dimensions. This resistance allows to distribute physically the heat source towards the two elements without assumption on a possible partition coefficient (9).

In (10), REBs are supposed isothermal and are modelled with a single node. Neurouth *et al.* (15) developed a complex bearing model discretizing a bearing in 10 nodes within the FZG thermal modelling. They highlighted the difference of temperature between inner and outer rings. This temperature gradient in the bearing influences gear temperature. To model the temperature gradient a simplified approach (Figure 12) is implemented following Niel *et al.* (16) modelling strategy. Thus, each REB is discretized by four nodes: external and internal ring, rolling elements, and grease (Figure 12).

For lubricated condition, gear power loss is applied to the mesh element of the thermal network given in Figure 12. The model given by the standard (ISO 14179-2) (18) is used:

$$_{gears} = \ _{m} H_v f_{mean} \qquad [1]$$

- $_{m}$: mechanical power (W)
- H_v: form factor depending on gear geometry (-)
- f_{mean}: Mean friction coefficient along line of action (-)

The friction coefficient along the action line is calculated with the formulation of Castro and Seabra (4). This one is based on Winter and Michaelis equation (5) and was derived from experimental FZG C type gear tests (5).

$$\mu^{FZG}(x) = 0.257 \frac{(x)^{0.18}}{V_R(x)^{0.26}} \eta_0{}^{-0.05} \left(\frac{R_a}{d_p}\right)^{0.25} \quad [2]$$

- (x) : Hertzian pressure along line of action (GPa)
- $V_R(x)$: Rolling speed along line of action (m.s-^{1})
- R_a: Arithmetic mean height of roughness (µm)
- d_p: Pitch diameter (mm)
- η_0: Oil dynamic viscosity (mPa.s)

$$f_{mean} = \frac{\int_A^B \mu^{FZG}(x).N(x).V_s(x)\,dx}{\int_A^B N(x).V_s(x)\,dx} \quad [3]$$

- A, B: Beginning, end of line of action
- N(x) : Normal force along line of action (N)
- $V_s(x)$: Sliding speed along line of action (m.s-^{1})

The REB power losses (6306-2RS1) are applied to the central element of each REB (Figure 12). This power loss is modelled with SKF model (19) formalized as:

$$M = M_{rolling} + M_{sliding} + M_{seals} + M_{drag} \quad [4]$$

Where $M_{rolling}$ and $M_{sliding}$ are loss torque respectively induced by rolling and sliding phenomenon. M_{seals} is loss torque by friction between seals and rings. M_{drag} is the loss torque due to drag of rolling elements moving throughout oil.

Seal power losses are applied to the shaft elements of the thermal network. They are estimated considering Freudenberg formulation (20):

$$_{seal} = 7.69.10^{-6}.n.d^2\omega \quad [5]$$

- n: number of lips (-)
- d: shaft diameter (mm)
- ω: shaft rotational speed (rpm)

Churning power losses are applied to the oil bath node (Figure 12) during oil bath lubrication using Changenet *et al*. model (9):

$$_{\text{churning}} = \frac{1}{2}\rho_{oil} S_m {R_p}^3 \omega^3 C_m \quad [6]$$

- ρ_{oil}: Oil density ($kg.m^{-3}$)
- S_m : Submerged surface (m^2)
- R_p: Pitch radius (m)
- ω : Rotational speed ($rad.s^{-1}$)
- C_m: Dimensionless drag coefficient defined by LePrince *et al*. (21) to take oil aeration into account

The power loss decrease observed in Figure 13 is strongly linked to the decrease of oil viscosity during temperature rise. Operating temperatures of the system are themselves driven by heat generations. Numerical power loss (Figure 13) and temperatures (Figure 14) are representative of their experimental counterparts. In these figures, marks represent the experimental findings whereas lines are associated with the numerical ones. This means the strong coupling between heat generations and temperatures is accurately performed. This coupling will be all the more important for the modelling of starvation conditions that implies severe temperature variations (Figure 9).

Numerical method to estimate power loss variation during a starvation test

Firstly, the thermal modelling of the FZG is modified to consider starved conditions. In fact, these conditions imply modifications on heat exchanges within the system. The oil bath node

is replaced with the internal air. The gear rotation generates internal air flow responsible for forced convection with housing internal surfaces and gear flanks. The heat transfer coefficient applied on housing surfaces is estimated using the following formulation of the Nusselt number corresponding to the case of flows over flat plates (22):

For

$R_e < 5.10^5$ $$N_u = 0.664\, R_e^{1/2}\, {}_r^{1/3}$$ [7]

Else

$R_e \geq 5.10^5$ $$N_u = {}_r^{\frac{1}{3}}(0.037\, R_e^{4/5} - 850)$$ [8]

The heat transfer coefficient applied on gear flanks is estimated using the following formulation of the Nusselt number corresponding to the case of a disk rotating in a motionless fluid (10):

$R_e < 2.5.10^5$ $$N_u = 0.4\, R_e^{1/2}\, {}_r^{1/3}$$ [9]

$R_e > 3.2.10^5$ $$N_u = 0.238\, R_e^{0.8}\, {}_r^{0.6}$$ [10]

With

$$R_e = \frac{V_\infty L_{cara}}{\nu_{air}}$$ [11]

- $V_\infty = R_p \omega$: tangential speed ($m.s^{-1}$) [12]
- R_p: Pitch radius (m)
- ω: Rotational speed ($rad.s^{-1}$)
- $\nu_{air} = 15.6.10^{-6}$ $(kg.m^{-1}.s^{-1})$
- L_{cara} : Characteristic length (m)

${}_r = 0.7$ for dry air and assumed constant versus temperature

REBs are greased and sealed to prevent starvation. Power loss in seals is considered as constant. Without oil bath, the churning loss is suppressed and the windage power loss is neglected because of the small dimensions and low operating speeds. Figure 15 is a diagram describing a numerical method to estimate the variation of gear power losses during a starvation test. P_{Gears} is the power loss applied to gear. P_{lub} is the gear power losses under lubricated condition used as initial power loss value. In this case, a mean friction coefficient of 0.03 was calculated with equation 3 that corresponds to a power loss of 160 W (equation 1). $_{exp}$ is the experimental power loss of the test box determined with the experimental method presented in part 4 (Figure 11) . $_{num}$ is the sum of all power loss sources calculated in the thermal network. ε is the precision desired on the solution (here $\varepsilon = 1$ W).

As expected, the numerical total power loss of the test box is accurately determined by the method for 4 iterations (Figure 16). Figure 17 presents correlation between experimental and numerical temperatures. The thermal modelling is able to predict the global variations of temperature during the starvation test. It should be noticed a severe increase of the pinion bulk temperature between 2.5 and 3 min. Further experimental analyses show scuffing. This phenomenon induced local and transient thermal elevations. This specific model cannot predict it as gears are assumed to be isothermal.

The main hypothesis of the method is that only gear power losses are impacted by starvation. To verify this assumption, the power loss increase due to starvation is numerically assigned to seals. Gear power loss is modelled using equation [1] by considering it was not affected by starvation conditions. Extra seal power loss is obtained by adapting the method described in Figure 16. At initialisation step, seal power loss value is calculated using equation [5]. For each iteration, ΔP is added to seal power loss until experimental power loss is reached. This calculated power loss is shared between the four seals of the test box considering account their rotational speed. Indeed, according to equation [5], seals associated to the secondary

shaft dissipate 1.5 times more than those mounted on the primary one. Figure 18 highlights differences between numerical and experimental temperatures for this modelling. It confirms that the power loss increase during starvation occurs for gears.

Figure 19 presents gear power loss variations during starvation tests. A severe increase more than 900 W that represents a rise of 575 % concerning gear power loss is observed after 3 min 20 s of starvation test. However, focusing on experimental power loss values, the variation observed between lubricated and starved condition is 800 W (part 4, Figure 11). To explain this difference, Figure 20 draws up the variation power loss source distribution for lubricated and starved condition tests. For the lubricated condition, a low variation is observed during 3 minutes because the thermal kinetics is very slow. However, under starved conditions, thermal kinetics is quick because of the severe increase of gear tooth friction losses. A decrease of 100 W is observed, by adding variations of bearing and churning losses comparing a lubricated and a starved test. These are actually dissipated by gears. This highlights the importance of a model including a strong coupling between temperatures and heat generations.

Conclusion and perspective

The aim of this paper was to study the impact of starved lubrication conditions on gear power loss. Firstly, the FZG test rig and the operating conditions were described. In the second part, an experimental method to isolate power loss of the test box was proposed. The torque loss of the slave box was characterized from test performed with the FZG test rig for a symmetrical configuration. This torque is used to isolate the test box power loss during starvation tests. To perform these last ones, modifications of the FZG test rig and a specific procedure were presented. The main conclusions linked to the tests are:

- Thermal kinetics is severely accelerated under starved conditions. An increase of more than 60 °C on gear bulk temperatures is measured after 3 minutes which corresponds to an increase of more than 190%.

- Power losses of the system increase significantly during starvation. An increase of 800 W is observed after 3 minutes that represents an increase of 60 % in comparison with nominal lubricated conditions.

To analyze the dissipation sources with this power loss evolution, a thermal model of the test rig is proposed. This model, based on thermal network method, allows a strong coupling between power losses and temperatures. For a starvation context involving severe temperature variations, this coupling is essential to estimate accurately gear power loss variations. These gear power loss increases are estimated using a semi-inverse method with the previous thermal model adapted to starved conditions. Gear power loss estimated thanks to the numerical model highlights a severe rise of 900 W during the starvation that represents an increase of 575 %

In sight, determination of gear power loss variations during starvation allows to go further in the field of starvation conditions. In fact, works oriented to starved contact behaviour may be undertaken. For instance, film thickness reduction analyses may be performed based on an expansion of the semi-inverse method. This analysis could lead to predict scuffing under starved conditions.

Acknowledgments

The authors disclosed receipt of the following financial support for the research, authorship, and/or publication of this article. The authors would like to thank the ANRT (CIFRE n°2018/0789).

Nomenclature

Symbol	Name	Unit
a	Center distance	(mm)
A, B	Beginning, end of the meshing	(-)
b	Gear and REB widths	(mm)
C	REB dynamic load	(kN)
C_0	REB static load	(kN)
C_m	Dimensionless drag coefficient	(-)
d	shaft diameter	(mm)
D	External REB diameter	(mm)
d_a	Addendum diameter	(mm)
d_p	Pitch diameter	(mm)
f_{mean}	Mean friction coefficient along the action line	(-)
H_v	form factor depending on gear geometries	(-)
L_{cara}	Characteristic length	(m)
m	Module	(mm)
M	Total torque loss of REB	(N.mm)
$M_{sliding}$	Torque loss due to sliding for REB	(N.mm)
$M_{rolling}$	Torque loss due to rolling for REB	(N.mm)
M_{seals}	Torque loss due to seals for REB	(N.mm)
M_{drag}	Torque loss due to drag for REB	(N.mm)
n	Number of lips for seals	(-)
N(x)	Normal force along action line	(N)
N_u	Nusselt number	(-)
r	Prandtl number	(-)

$P_{churning}$	Churning power loss	(W)
P_{seal}	Seal power loss	(W)
P_{gears}	Gear power loss	(W)
P_{lub}	Gears power loss under lubricated regime	(W)
P_{num}	Numerical total power loss	(W)
$p(x)$	Hertzian pressure along action line	(GPa)
P_m	mechanical power	(W)
R_a	Arithmetic mean height of roughness	(µm)
R_e	Reynolds number	(-)
R_p	Pitch radius	(m)
S_m	Submerged surface	(m^2)
V_∞	Tangential speed	($m.s^{-1}$)
$V_R(x)$	Rolling speed along action line	($m.s^{-1}$)
$V_s(x)$	Sliding speed along action line	($m.s^{-1}$)
x	Profile shift modification	(-)
Z	Teeth number	(-)
α	Pressure angle	(°)
β	Helix angle	(°)
ε	Precision	(W)
η_0	Oil dynamic viscosity	(mPa.s)
ν_{air}	Air kinematic viscosity	(mm^2/s)
ν_T	Oil kinematic viscosity	(mm^2/s)
$\mu^{FZG}(x)$	Friction coefficient along the meshing line	(-)
ρ_{oil}	Oil density	($kg.m^{-3}$)

References

(1) Höhn, B.R., Michaelis, K. and Völlmer, T. (1996), "Thermal rating of drives: balance between power loss and heat dissipation," AGMA technical paper 96FTM08. Alexandria, VA: American Gear Manufactures Association, p 12.

(2) Andersson, M., Sosa, M. and Olofsson, U. (2017) 'Efficiency and temperature of spur gears using spray lubrication compared to dip lubrication', Proceedings of the Institution of Mechanical Engineers, Part J: Journal of Engineering Tribology, **231**(11), pp. 1390–1396.

(3) Fernandes, C., Marques, P., Matins, R.C. and Seabra, J. (2014), "Gearbox power loss. Part II: Friction losses in gears," Tribology International, **88**, pp 309-316.

(4) Höhn, B.R., Michaelis, K. and Doleschel A. (2001), "Frictional behaviour of synthetic gear lubricants," Dalmaz G, editor, Tribology research:from model experiment to industrial problem. Amsterdam: Elsevier Science B.V., pp 759–68.

(5) Winter, H. and Michaelis, K. (1993), "Scoring load capacity of gears lubricated with, ep-oils," AGMA, Fall Technical Meeting, Technical paper no. pp 219-17, Montreal, Canada.

(6) Castro, J. and Seabra, J. (2008), "Global and local analysis of gear scuffing tests using a mixed film lubrication model," Tribology International, **41**, pp 244-255.

(7) Matins, R.C., Cardoso, N.R., Bock, H., *et al*. (2009), "Power loss performance of high pressure nitrided steel gears," Tribology International, **42**(1), pp 1807-1815.

(8) Martins, R.C., Seabra J., Brito, A., *et al*. (2006), "FZG coefficient in FZG gears lubricated with industrial gear oils: Biodegradable ester vs. mineral oil," Tribology International, **39**(1), pp 512-521.

(9) Changenet, C., Oviedo-Marlot, X. and Velex, P. (2006), "Power loss predictions in geared transmissions using thermal networks – applications to a six–speed manual gearbox," J Mech Des, **128**, pp 618–625.

(10) Durand de Gevigney, J., Changenet, C., Ville, F., and Velex, P. (2012), "Thermal modelling of a back-to-back gearbox test machine: Application to the FZG test rig," Proceedings of the Institution of Mechanical Engineers, Part J: Journal of Engineering Tribology, **226**(6), pp 501–515.

(11) Chevalier, F., Lubrecht A.A., Cann, P.M.E., Colin, F. and Dalmaz, G. (1998), "Film Thickness in Starved EHL Point Contacts," Transactions of the ASME, **120,** pp 126 – 133.

(12) Damiens, B., Venner , C.H., Cann, P.M.E. and Lubrecht, A.A. (2006), "Starved Lubrication of Elliptical EHD Contacts," ASME Journal of Tribology, 2004, **126**, pp 105 – 111.

(13) Querlioz, E., Ville, F., Lenon, H., and Lubrecht, T. (2007), "Experimental investigations on the contact fatigue life under starved conditions," Tribology International, **40**, pp.1619-1626.

(14) Blok, H. (1970), "La méthode des réseaux thermique pour le calcul des températures de masse dans les transmissions à engrenages," Société d'études de l'industrie de l'engrenage, **59**, pp 3–13.

(15) Neurouth, A., Changenet, C., Ville, F. and Michel, M. (2017), "Influence of Rolling Element Bearing Modelling on the Predicted Thermal Behavior of the FZG Test Rig," Tribology Transactions, **60**(4), pp. 753-761.

(16) Niel, D., Changenet, C., Ville, F., and Octrue, M. (2019), "Thermomecanical study of high speed rolling element bearing: A simplified approach," Proceedings of the Institution of Mechanical Engineers, Part J: Journal of Engineering Tribology, **233**(4), pp 541–552.

(17) Meheux, M. et al. (2008) 'Influence of slide-to-roll ratio on tribofilm generation', Proceedings of the Institution of Mechanical Engineers, Part J: Journal of Engineering Tribology, **222**(3), pp. 325–334.

(18) ISO/TR 14179-2 (2001), "Gears, Thermal capacity".

(19) SKF *General Catalogue* (2005), 6000EN, SKF.

(20) Simrit, *Radialwellendichtringe*, Katalog Nr. 100.

(21) LePrince, G., Changenet, C., Ville, F., Velex, P., Dufau, C., and Jarnias, F. (2011), "Influence of Aerated Lubricants on Gear Churning Losses–An Engineering Model," Tribology Transactions, **54**(6), pp 929-938.

(22) Schlichting, H. (1979), *Boundary Layer Theory*, McGraw-Hill, 7th Ed., p. 817.

Torque transducer	Characteristics				
T22	Nominal Torque (N.m) 50	Voltage output (V) ± 5	Sensitivity on voltage (V) ± 0.2	Accuracy class 0.5	Absolute accuracy (N.m) 0.25

Table 1. Torque transducer characteristics

Gears		Parameters								
		Z (-)	m (mm)	a (mm)	α (°)	β (°)	b (mm)	x (-)	d_a (mm)	R_a (μm)
FZG C30	Pinion	16	4.5	91.5	20	0	30	0.1817	82.64	0.4
	Gear	24						0.1715	115.54	
FZG A20	Pinion	16	4.5	91.5	20	0	20	0.85	88.65	0.4
	Gear	24						-0.5	112.50	

Table 2. Parameters of gears

REB	Parameters					
	Seals	d (mm)	D (mm)	b (mm)	C (kN)	C_0 (kN)
6406	-	30	90	23	43.6	23.6
6306-2RS1	2xRS1	30	72	19	28.1	16

Table 3. Parameters of bearings

Oil	Parameters		
	Density at 40 °C ($kg.m^{-3}$)	$\nu_{40°C}$ (mm^2/s)	$\nu_{100°C}$ (mm^2/s)
IGOL HYPOID 85W-90	900	187	17.1
NYCOBASE 5750	987	24	5

Table 4. Oil parameters

Gears Parameters	Pinion torque (Nm)	Maximal normal load (N)	Maximal hertzian pressure (GPa)	Pinion Speed (rpm)	Input power (kW)
Operating condition 1	60.8	1800	0.65	3000	19

Table 5. Operating conditions

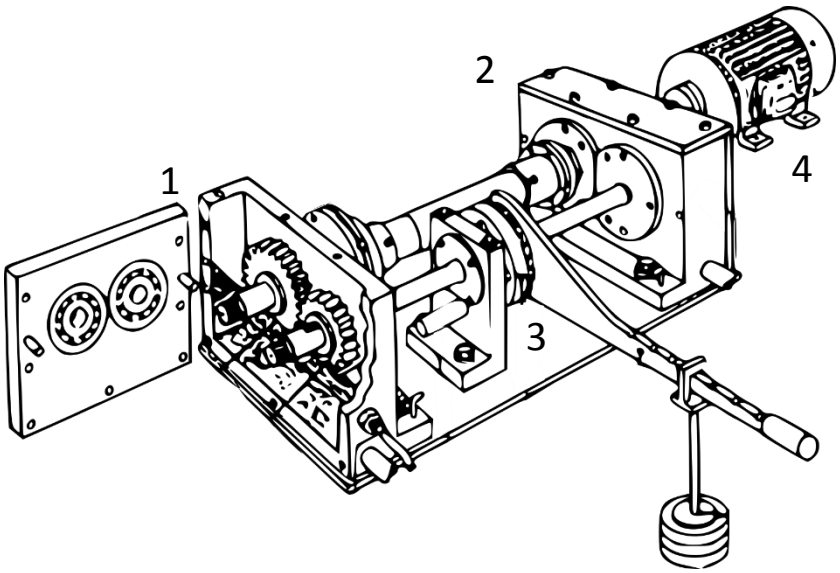

Figure 1. Drawing of a FZG test rig

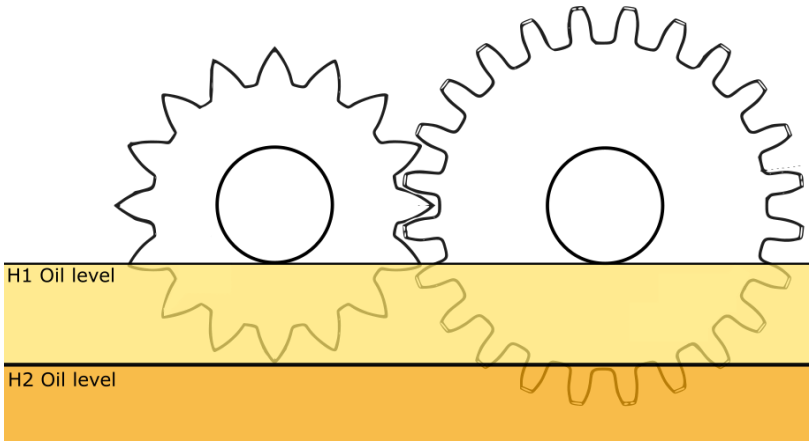

Figure 2. Oil levels

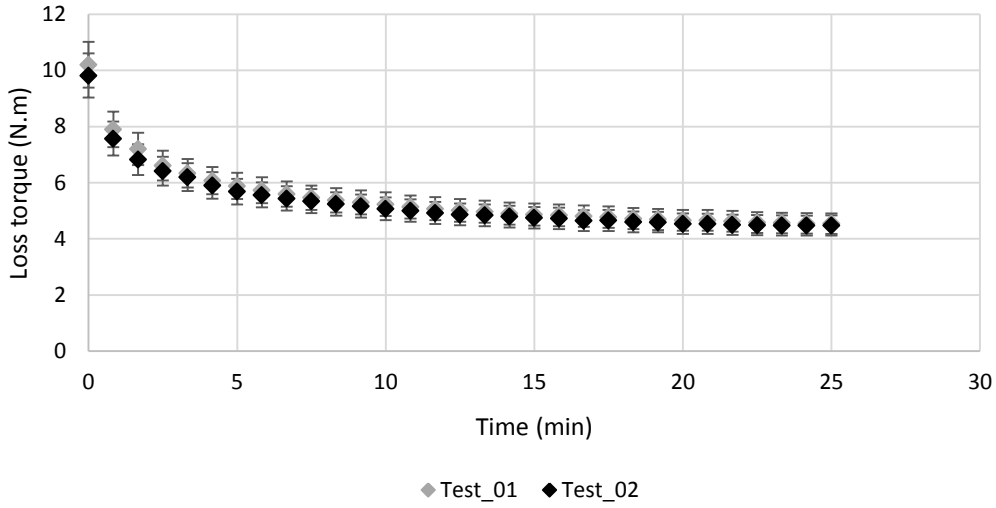

Figure 3. Repeatability of the total loss torque; operating condition 1

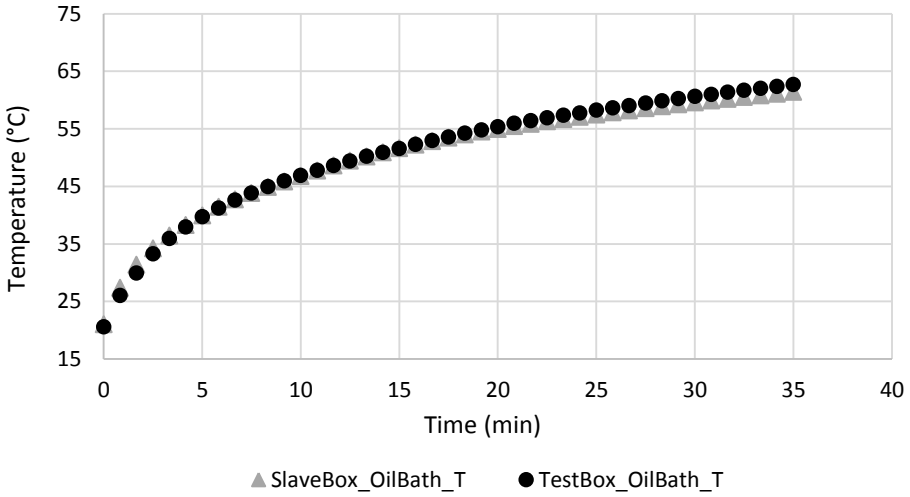

Figure 4. Oil bath temperatures; operating condition 1

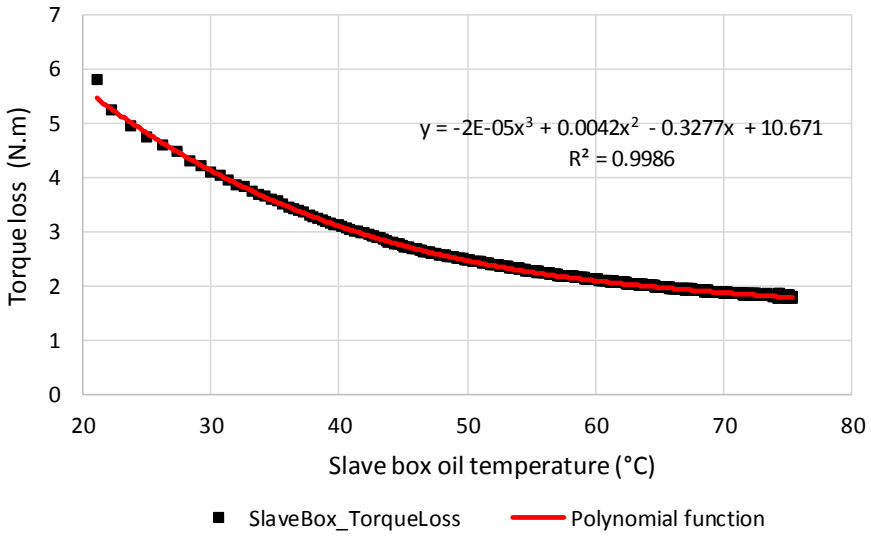

Figure 5. Slave box torque loss; operating condition 1

Figure 6. Thermocouple sensors stuck on gears tooth

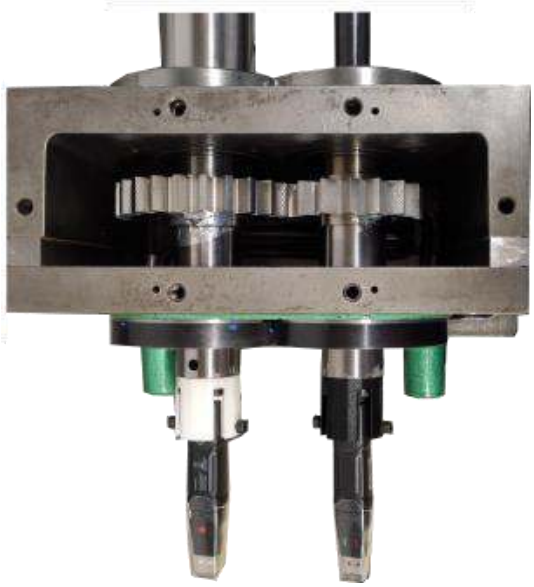

Figure 7. Test box equipped with data loggers

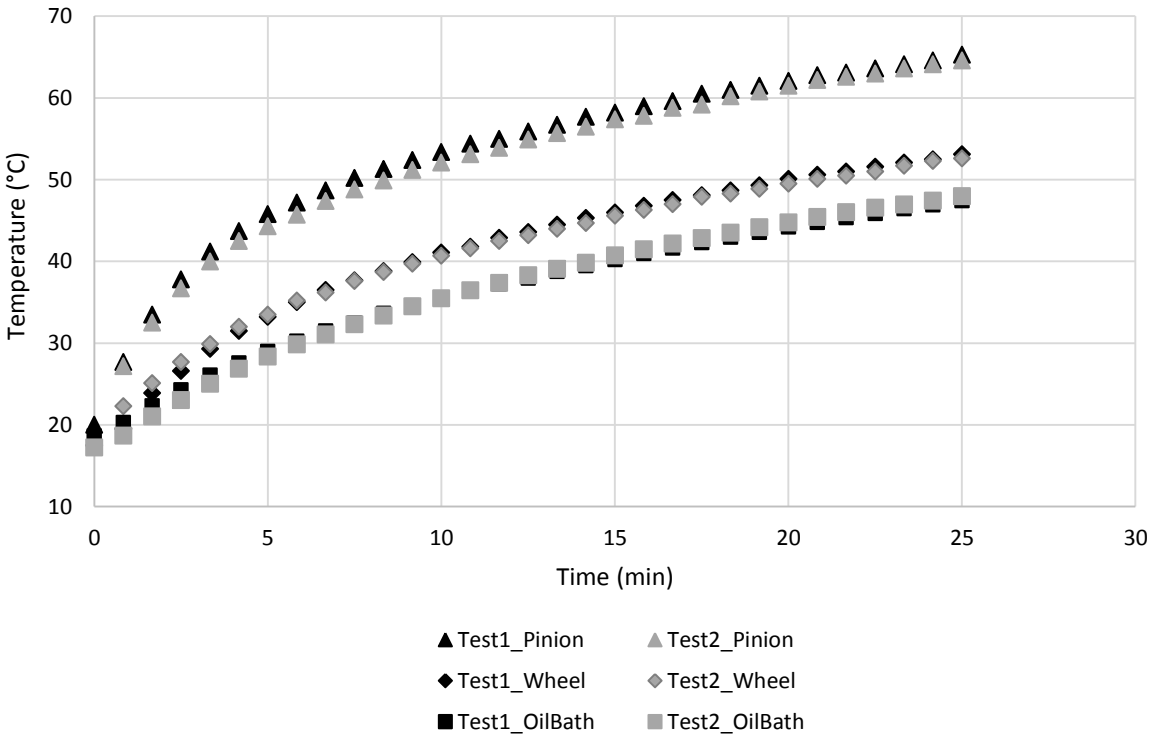

Figure 8. Repeatability of operating temperatures; operating condition 1

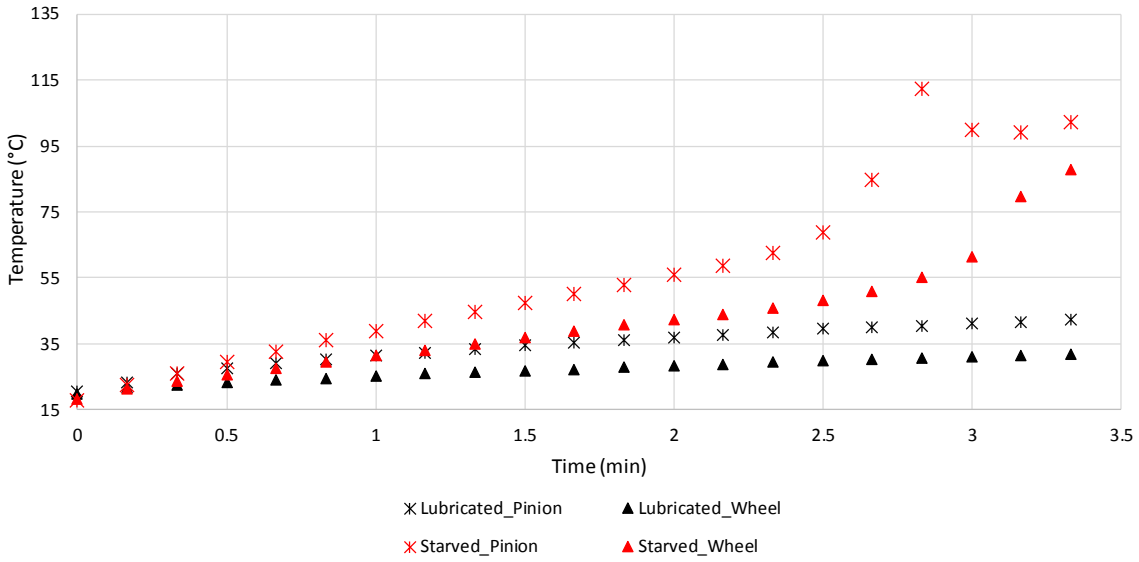

Figure 9. Gears embedded bulk temperature in lubricated and starved conditions; operating condition 1

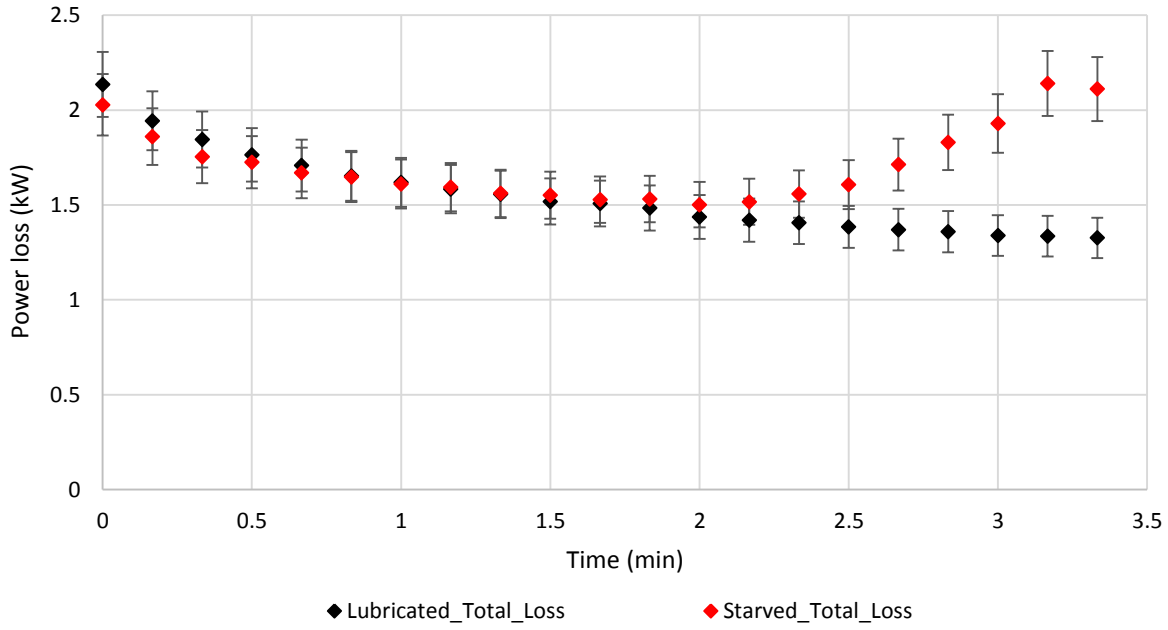

Figure 10. Total power loss during lubricated and starved conditions; operating condition 1

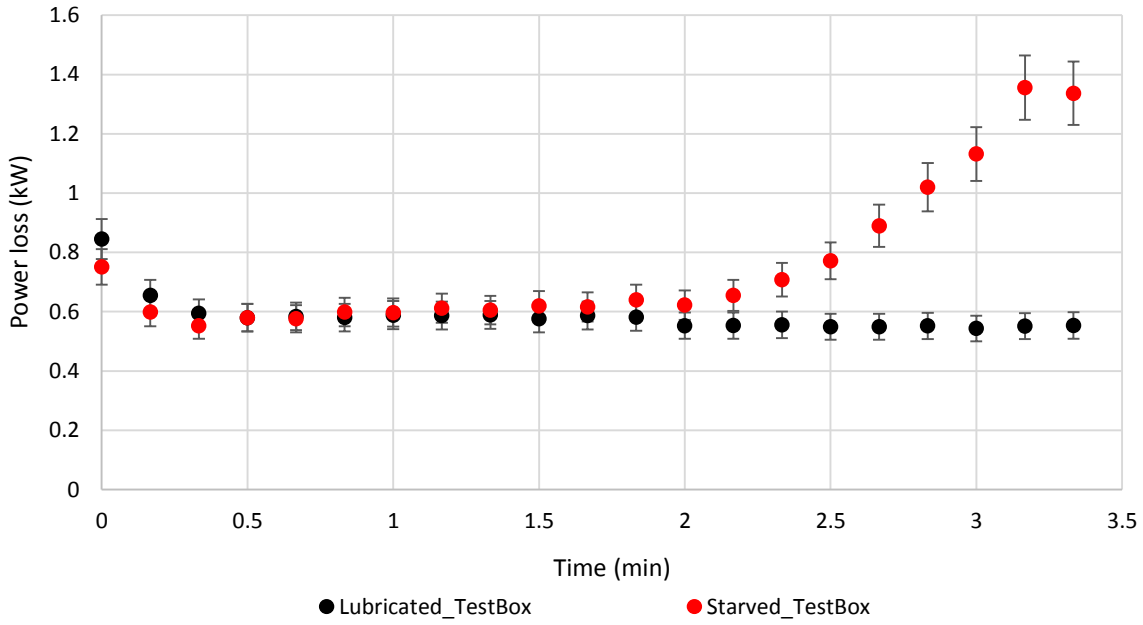

Figure 11. Power loss of the test box in lubricated and starved conditions; operating condition 1

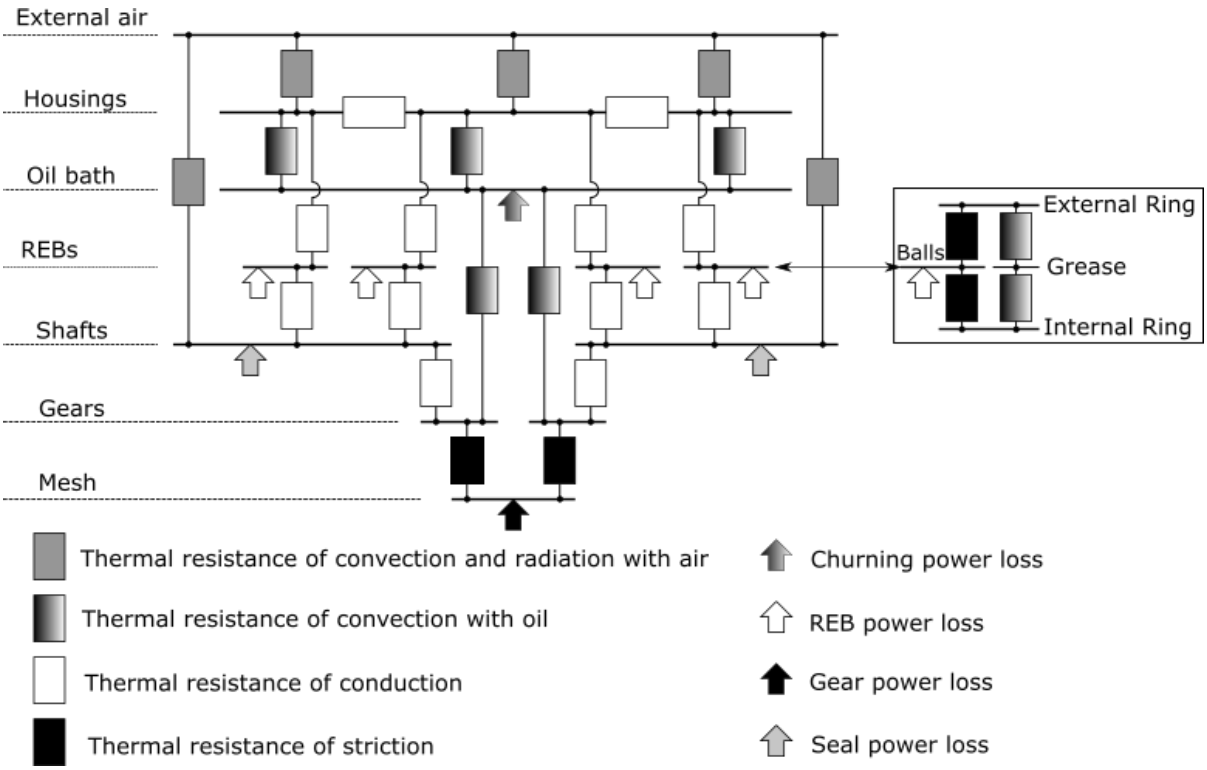

Figure 12. Thermal network of the FZG test rig

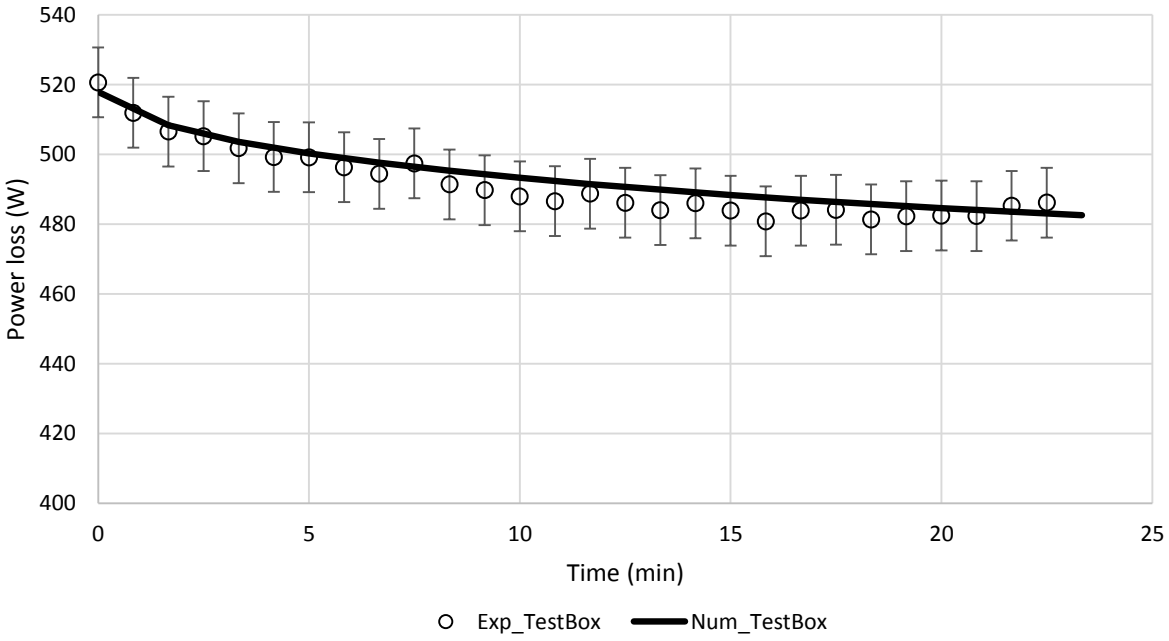

Figure 13. Numerical and experimental power loss of the test box; operating condition 1

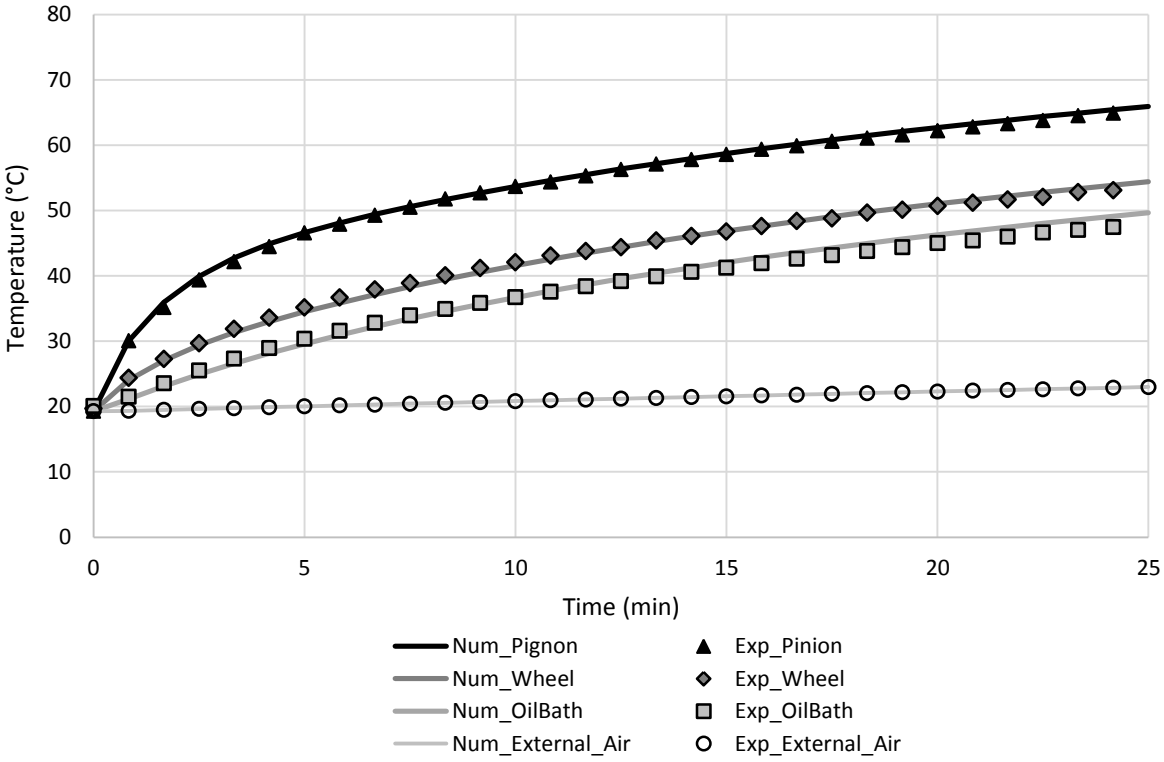

Figure 14. Numerical and experimental temperatures; operating condition 1

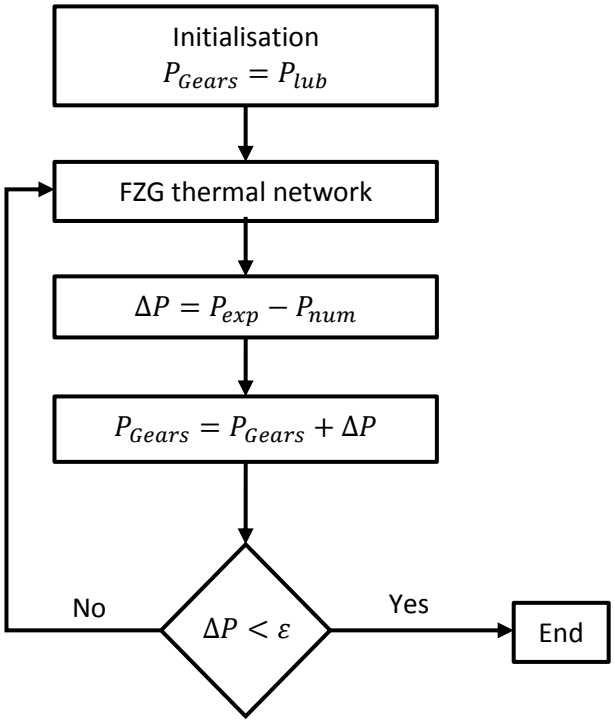

Figure 15. Method to estimate gears power loss during a starvation test

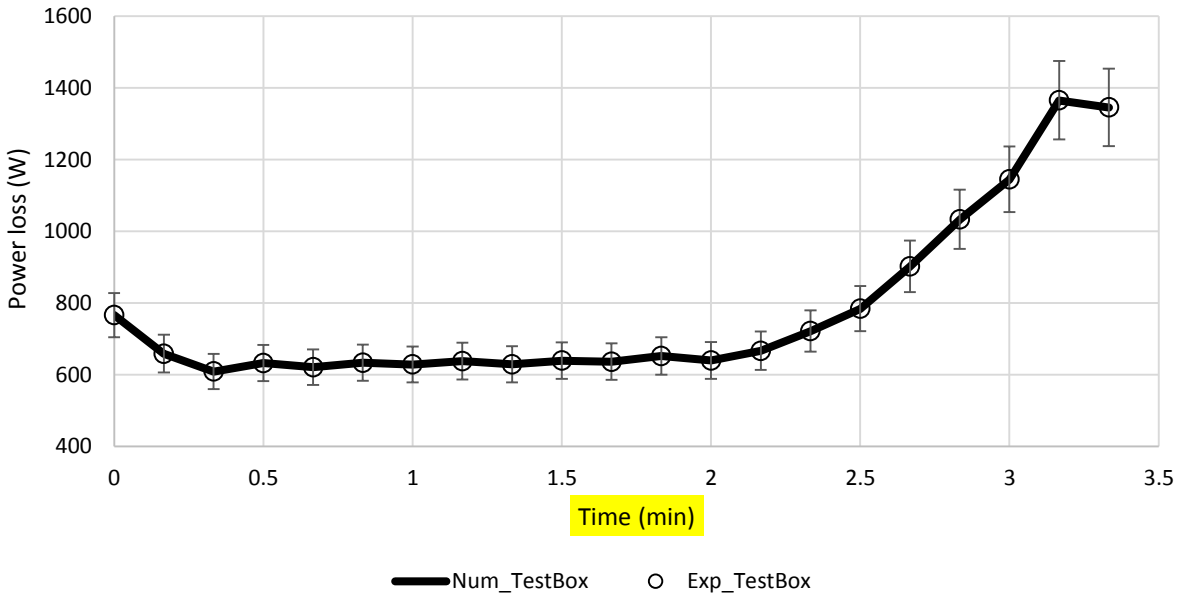

Figure 16. Numerical and experimental total power loss of the test box

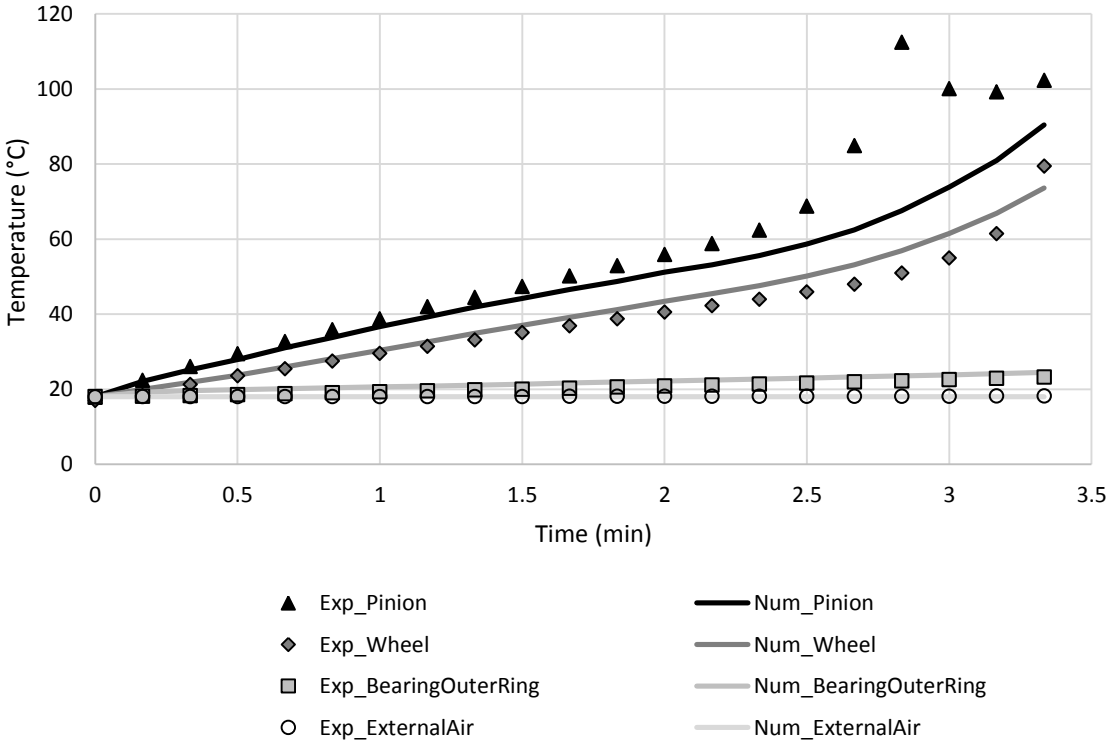

Figure 17. Experimental and numerical temperature in starved condition

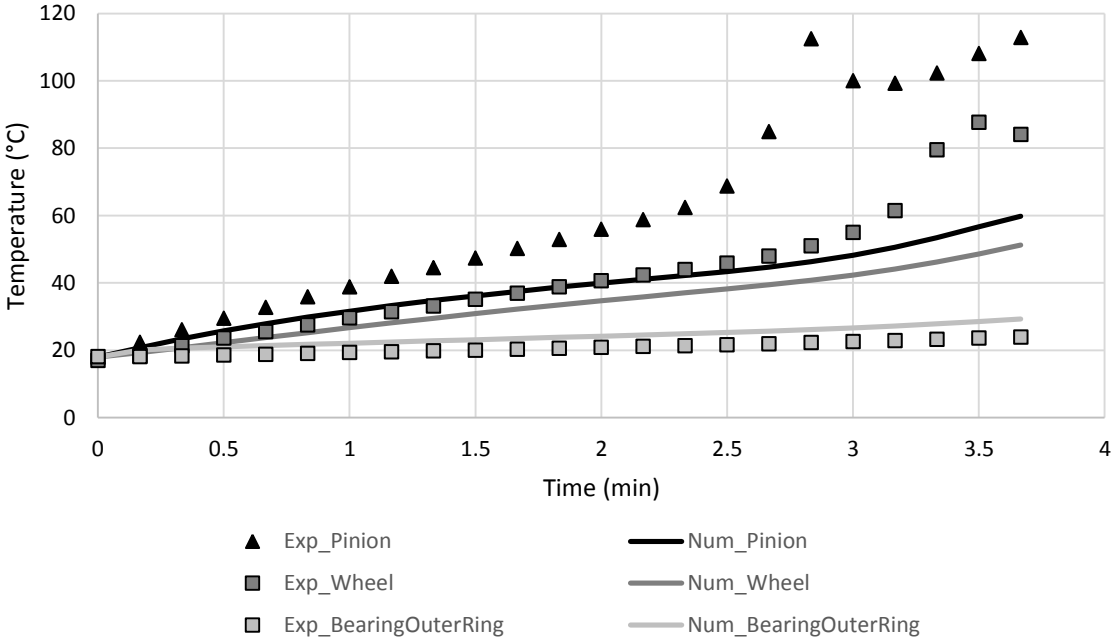

Figure 18. Numerical and experimental temperatures applying power losses increase on seals

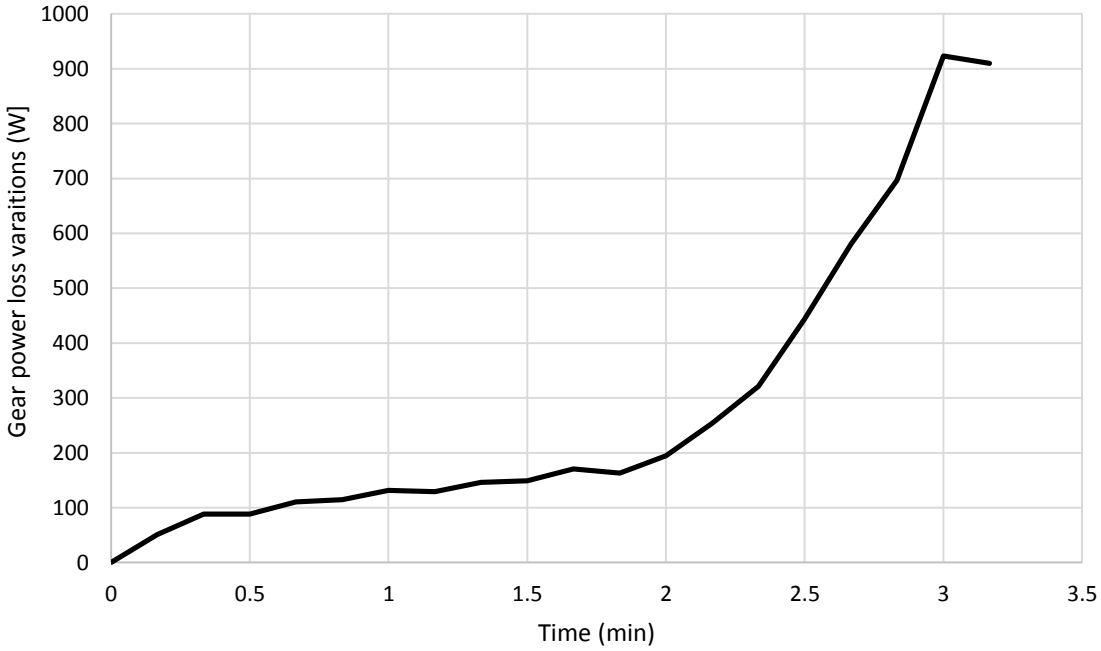

Figure 19. Increase of gears losses during a starvation test; operating condition 1

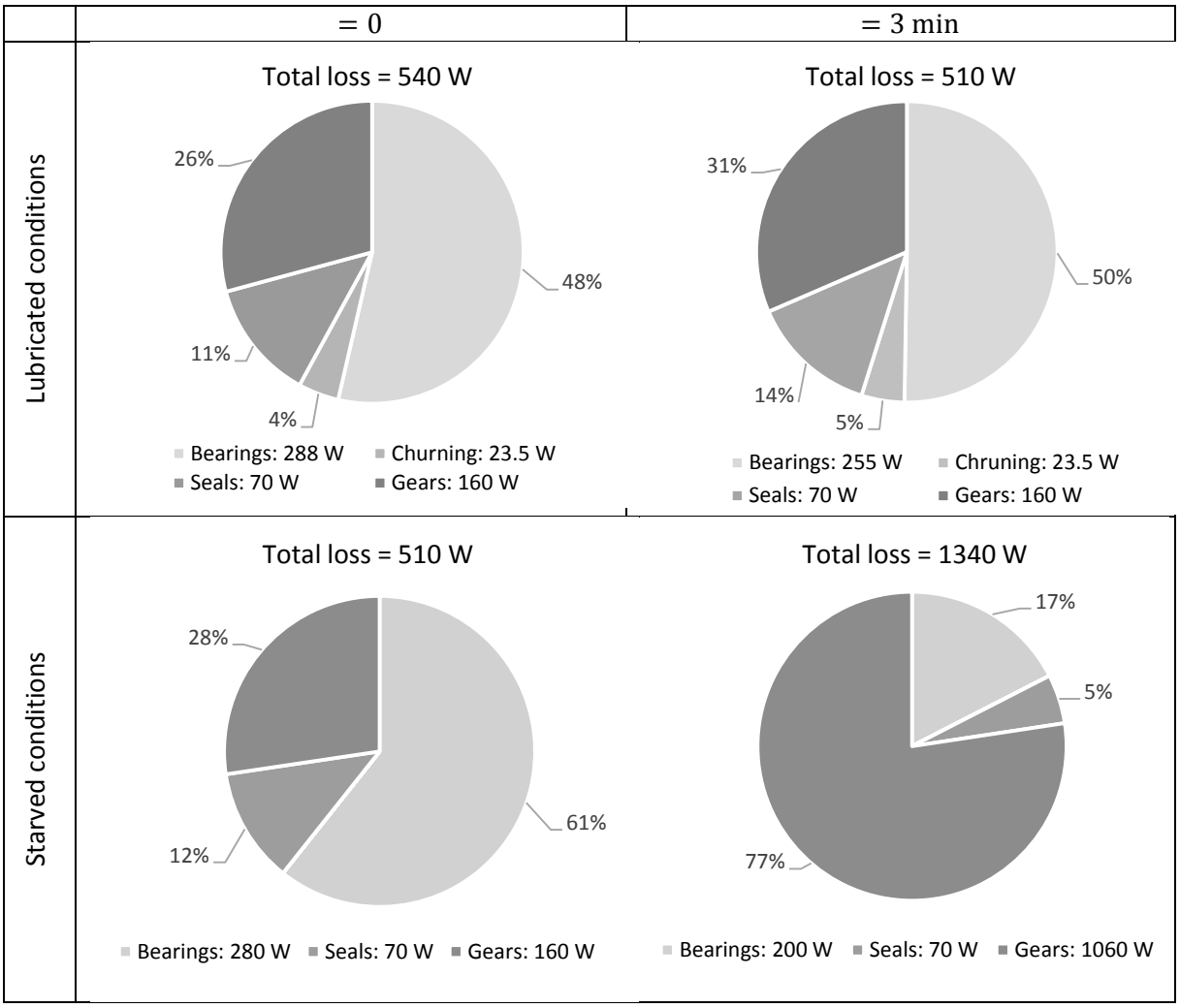

Figure 20. Distribution of power loss sources